B_c meson production in $\gamma\gamma$ collisions and charm content of the photon

A.P.Martynenko and V.A. Saleev

Samara State University, Samara, 443011, Russia

Abstract

Based on photon structure function formalism we have calculated $B_c(B_c^*)$ meson production cross section in $\gamma\gamma$ collisions via partonic subprocess $c\gamma \to B_c(B_c^*)b$. It was shown that this approach gives the same results for $B_c^*(B_c)$ meson cross sections as the direct leading order QCD calculation of the subprocess $\gamma\gamma \to B_c(B_c^*)b\bar{c}$ at small energy. Howere, opposite to the direct QCD calculation we have obtained the increase of the $B_c(B_c^*)$ meson cross section at large energies. We have found also additional contribution to the B_c meson production via the nonperturbative fluctuations $\gamma \leftrightarrow J/\psi$.

The recent measurements at HERA *ep* collider [1] shown nontrivial role of the photon structure function (PSF) [2] in photoproduction of jets and charm quarks at high energies. Usually it is supposed that the gluon content of the photon in the resolved photon interaction is dominant at high energies [3]. However, the charm content of the photon may be also very important for processes of charm photoproduction as well as the charm content of the proton for charm hadroproduction processes. First of all, the hadron-like (nonperturbative) charm quark contribution is needed for description of the large diffractive charm production [4]. At second, the many aspects of charm production in the hard processes, where QCD scale parameter Q^2 is large ($Q^2 >> m_c^2$), can be understood in the context of perturbative QCD as a initial state charm excitation processes [5]. Recently, we have calculated the cross sections of the J/ψ photo- and hadroproduction at the large transverse momentum via charm quark excitation in proton [6] and photon [7]. In the present paper we discuss the contribution of the charm quark PSF in the $B_c(B_c^*)$ meson production via partonic subprocess $\gamma c \to B_c(B_c^*)$ in $\gamma\gamma$ collisions. Because of the QCD scale parameter Q^2 in this process is order to square of B_c meson mass ($Q^2 \approx M_{B_c}^2 >> m_c^2$), the application of the c-quark PSF approach for $B_c(B_c^*)$ meson production is well grounded as for calculation of the large $p_\perp$ B_c meson production as for the calculation of the total cross section. Taking into account the mass of the initial c-quark in the kinematic relations as well as in the c-quark distribution functions, we can control the mass corrections near the threshold of the B_c meson production.

The production mechanisms for $B_c(B_c^*)$ mesons in $\gamma\gamma$ collisions have been discussed early in Refs. [8, 9]. It was assumed that in $\gamma\gamma$ collision $B_c(B_c^*)$ mesons are dominantly produced in association with a b- and c- quark jets via the partonic subprocess:

$$\gamma + \gamma \to B_c(B_c^*) + b + \bar{c}, \tag{1}$$

which is described by twenty Feynman diagrams. In this paper, we examine a B_c and B_c^* meson production via the partonic subprocess:

$$c(q) + \gamma(k) \to B_c(P) + b(q_1). \tag{2}$$

The above subprocess is described only by four Feynman diagrams which are shown in Fig.1. The corresponding amplitudes can be expressed as follows:

$$\mathcal{M}_1 = e_b e g^2 T^a T^a \bar{U}_b(q_1)\hat{\varepsilon}_\gamma(k)\frac{\hat{q}_1 - \hat{k} + m_b}{(q_1-k)^2 - m_b^2}\gamma_\rho \frac{\hat{\Pi}}{(p_c-q)^2}\gamma^\rho U_c(q) \tag{3}$$

$$\mathcal{M}_2 = e_c e g^2 T^a T^a \bar{U}_b(q_1)\gamma_\rho \frac{\hat{\Pi}}{(p_b+q_1)^2}\gamma^\rho \frac{\hat{k} + \hat{q} + m_c}{(q+k)^2 - m_c^2}\hat{\varepsilon}_\gamma(k) U_c(q) \tag{4}$$

$$\mathcal{M}_3 = e_c e g^2 T^a T^a \bar{U}_b(q_1)\gamma_\rho \frac{\hat{\Pi}}{(p_b+q_1)^2}\hat{\varepsilon}_\gamma(k)\frac{\hat{p}_c - \hat{k} + m_c}{(p_c-k)^2 - m_c^2}\gamma^\rho U_c(q) \tag{5}$$

$$\mathcal{M}_4 = e_b e g^2 T^a T^a \bar{U}_b(q_1)\gamma_\rho \frac{\hat{k} - \hat{p}_b + m_b}{(k-p_b)^2 - m_b^2}\hat{\varepsilon}_\gamma(k)\frac{\hat{\Pi}}{(p_c-q)^2}\gamma^\rho U_c(q) \tag{6}$$

Here, $\bar{U}_b(q_1)$ and $U_c(q)$ denote the Dirac spinors of the quarks, $T^a = \lambda^a/2$, $e = \sqrt{4\pi\alpha}$, $g = \sqrt{4\pi\alpha_s}$, e_c and e_b are electric charges of the quarks in units of e, m_c and m_b are quark masses, $\varepsilon_\gamma(k)$ is the photon polarization four-vector. The spin and colour properties of the $\bar{b}c$ ground state are described in nonrelativistic approximation by following projection operator [10]:

$$\hat{\Pi} = \frac{F_c \Psi(0)}{2\sqrt{M}} \hat{a}(\hat{P} + M), \tag{7}$$

where $F_c = \delta^{kr}/\sqrt{3}$, k and r are colour indexes of $\bar{b}-$ and $c-$ quarks, $M = m_c + m_b$ is B_c meson mass, $p_c = \frac{m_c}{M} P$ and $p_b = \frac{m_b}{M} P$ are $c-$ and $\bar{b}-$ quarks four-momenta, $P = p_c + p_b$ is B_c meson four-momentum, $\hat{a} = \gamma_5$ for pseudoscalar $\bar{b}c$ ground state and $\hat{a} = \hat{\varepsilon}$ for vector $\bar{b}c$ ground state. The $\Psi(0)$ is a nonrelativistic wave function at the origin which can be presented by the corresponding decay constants:

$$f_{B_c} = f_{B_c^*} = \sqrt{\frac{12}{M}} \Psi(0). \tag{8}$$

We put in our calculation: $f_{B_c} = f_{B_c^*} = 0.57$ GeV, $\alpha_s = 0.2$, $\alpha = 1/137$, $m_c = 1.5$ GeV and $m_b = 4.8$ GeV.

After average and sum over spins and colours of initial and final particles, we have obtained for square of matrix element:

$$\overline{|\mathcal{M}|^2} = B_{\gamma c} \sum_{i,j=1}^{4} e_i e_j F_{ij}(\hat{s}, \hat{t}, \hat{u}), \tag{9}$$

where

$$B_{\gamma c} = \frac{16}{27} \pi^3 \alpha \alpha_s^2 f_{B_c}^2,$$

$e_1 = e_4 = e_b$, $e_2 = e_3 = e_c$, $\hat{s} = (k+q)^2$, $\hat{t} = (k - q_1)^2$, $\hat{u} = (q - q_1)^2$ and $\hat{s} + \hat{t} + \hat{u} = m_c^2 + m_b^2 + M^2$. The explicit analytical formulae for functions F_{ij} are obtained using the symbolic manipulation program FORM [11] and automatically implemented into a FORTRAN program.

The differential cross section for subprocess $c\gamma \to B_c(B_c^*)b$ can be written as follows:

$$\frac{d\hat{\sigma}}{d\hat{t}} = \frac{\overline{|\mathcal{M}|^2}}{16\pi(\hat{s} - m_c^2)^2}. \tag{10}$$

For description of the $B_c(B_c^*)$ meson photoproduction via charm quark PSF we can use a conventional parton model. In this approach the measurable cross section is obtained by folding the hard parton level cross section with the respective parton densities:

$$\sigma(\gamma\gamma \to B_c X) = \int_{x_{min}}^{x_{max}} dx C_\gamma(x, Q^2) \int_{\hat{t}_{min}}^{\hat{t}_{max}} \frac{d\hat{\sigma}}{d\hat{t}}(c\gamma \to B_c b), \tag{11}$$

where $C_\gamma(x, Q^2)$ is a charm quark distribution of a photon,

$$\hat{t}\,_{min}^{max} = m_b^2 - \frac{\hat{s} - m_c^2}{2\hat{s}} [\hat{s} + m_b^2 - M^2 \pm \sqrt{(\hat{s} - (m_b + M)^2)(\hat{s} - m_c^2)}],$$

$$\hat{s} = x s_{\gamma\gamma} + m_c^2, \tag{12}$$

$$x_{min} = 4 m_b M / s_{\gamma\gamma}, \qquad x_{max} = Q^2/(Q^2 + 4m_c^2)$$

and $s_{\gamma\gamma}$ is the square of a total energy of photons in the $\gamma\gamma$ center-of-mass reference frame.

The charm content of a photon can be presented as the composition of a hadron–like PSF and a point–like (quark-gluon) PSF [2]:

$$C_\gamma(x, Q^2) = C_\gamma^{had}(x, Q^2) + C_\gamma^{pl}(x, Q^2). \tag{13}$$

In accordance with the vector-meson-dominance (VDM) model [12], the hadron–like c-quark PSF is presented via the charm quark distribution function of J/ψ meson:

$$C_\gamma^{had}(x, Q^2) = k \frac{4\pi\alpha}{f_\psi^2} C_\psi(x, Q^2) \tag{14}$$

with $1 \leq k \leq 2$. The precise value of k clearly has to be extracted from experiment. Similar to Ref.[13], where the photoproduction of charm hadrons in VMD model have been discussed, we used for $C_\psi(x, Q^2)$ the simple scaling parametrization, which takes into account c-quark mass effects:

$$C_\psi(x) = 49.5x^{2.2}(1-x)^{2.45}. \tag{15}$$

The c-quark point-like part of the PSF can be calculated using perturbative approach. As it was shown in Ref.[12], the distribution of a heavy quark with mass m_q in the photon near the threshold ($\sqrt{s_{\gamma\gamma}} \geq 2m_q$) should be calculated from the complete massive leading order (LO) Bethe - Heitler cross section for $\gamma^*\gamma \to q\bar{q}$ reaction:

$$C_\gamma^{pl}(x, Q^2) = \frac{3\alpha}{2\pi} e_c^2 F(x, \frac{m_c^2}{Q^2}), \tag{16}$$

where

$$F(x,r) = \beta[-1 + 8x(1-x) - 4rx(1-x)] + \\ [x^2 + (1-x)^2 + 4rx(1-3x) - 8r^2x^2]\ln[(1+\beta)/(1-\beta)],$$

$$\beta = \sqrt{1 - 4rx/(1-x)}.$$

Recently, the next leading order (NLO) corrections for the c-quark PSF was computed in Ref. [14]. Effectively, the point-like part of the $c-$quark PSF may be presented as a sum of Bethe – Heitler formula (16) (parametrization BH) and, so-called hadronic component [14], which corresponds to $c-$quark production via QCD evolution of the PSF.

In the Fig.2 c-quark PSF's are presented at scale $Q^2 = M^2$. The shapes of the curves for VMD and massive LO point-like parametrization (BH) are the same. Opposite these ones, point-like hadronic component of the $c-$quark PSF (parametrization PLH) increase at $x \to 0$. Below x about 0.01 the $c-$quark PSF is completely dominated by the point-like hadronic component. Obviously, that the following $x-$dependence gives the growth of the B_c meson $\gamma\gamma-$ production cross section at large $\sqrt{s_{\gamma\gamma}} >> M$.

The results of our calculation for B_c^* meson production cross section in $\gamma\gamma$ collisions as a function of $\sqrt{s_{\gamma\gamma}}$ are shown in Fig. 3. Curves 1 - 3 are the PSF contributions via subprocess $c\gamma \to B_c^* b$ with BH, VMD and PLH parametrization of PSF, respectively. Stars show the contribution of the direct production subprocess $\gamma\gamma \to B_c^* b\bar{c}$ and was taken from Ref.[8]. Note, that curve 2 was obtained at $k = 1$. One can see that BH parametrization of the c-quark PSF, based on the Bethe-Heitler formula, well coincides to the direct leading order QCD calculation from Ref.[8] as near the peak of the B_c^* meson production as near threshold, i.e. at $\sqrt{s_{\gamma\gamma}} = 15 \div 40$ GeV. The contribution of the hadron-like part of the c-quark PSF is about 30% (at $k = 1$) of the point-like part contribution at the $\sqrt{s_{\gamma\gamma}} = 15 \div 25$ GeV. At the large $\sqrt{s_{\gamma\gamma}}$ VMD contribution speedily decrease. Howere, if we take in mind, that for c-quarks as well as for light ones, it has from the experiment $k \approx 2$, we have obtained large additional contribution to the B_c^* - meson production via the nonperturbative fluctuations $\gamma \leftrightarrow J/\psi$.

The contribution of the point-like hadronic component is very small at $\sqrt{s_{\gamma\gamma}} \leq 50$ GeV. But at large energies the curve 3 demonstrates us nonfalling versus energy B_c^* meson production cross section. So, at $\sqrt{s_{\gamma\gamma}} = 100$ GeV the total resolved photon contribution five times the contribution of the direct production mechanism.

In Refs.[8, 9] the strong suppression of the pseudoscalar state production in comparison with the production of the vector one near threshold was obtained, so at $\sqrt{s_{\gamma\gamma}} = 15$ GeV $\sigma_{B_c^*}/\sigma_{B_c} \sim 55$[8] and at $\sqrt{s_{\gamma\gamma}} = 20$ GeV $\sigma_{B_c^*}/\sigma_{B_c} \sim 15$[8] or $\sigma_{B_c^*}/\sigma_{B_c} \sim 10$[9]. In spite of the fact that the results of our calculation for B_c^* meson production (Fig.3) at $\sqrt{s_{\gamma\gamma}} = 15 \div 40$ GeV are in agreement with Refs.[8, 9], the results for pseudoscalar B_c meson production are very different in this region of $\sqrt{s_{\gamma\gamma}}$. We have obtained that the $\sigma_{B_c^*}/\sigma_{B_c}$ ratio is approximately equal to 3 at all energies. We don't see the reason of strong additional suppression of the B_c meson production in comparison with B_c^* production near threshold in the partonic subprocesses $c\gamma \to B_c(B_c^*)b$.

The differential distributions of the B_c mesons in $\gamma\gamma$ collisions are also very interested. Figs. 4 and 5 show the spectra of B_c^* mesons versus the scaled energy variable $z = 2E_{B_c^*}/\sqrt{s_{\gamma\gamma}}$ obtained from the diagrams of the subprocess (2) at $\sqrt{s_{\gamma\gamma}} = 20$ GeV and $\sqrt{s_{\gamma\gamma}} = 100$ GeV, respectively. At small energy (Fig.4) the shapes of the $z-$spectra obtained using different parametrization are the same and the B_c^* meson production in the central region of z is dominant. The contribution of the point-like hadronic component at this energy is negligibly small. At high energy (Fig.5) the predictions of the discussed here $c-$quark PSF components are very different as for shape of the $z-$spectra as for the absolute values. The VMD and BH parametrizations predict two diffractive-like peaks both at $z \approx 0$ and $z \approx 1$ regions. The curve 3 (Fig.5) shows z-spectrum which was obtained using PLH parametrization. We see that the contributions of the pure photonic (BH) and hadronic (PLH) components of the PSF are dominant at different z and they may be separate experimentally.

Note, that the shape of the z-spectra in Figs.4 and 5 are remarkable different from result which was obtained in Ref.[9] using the model of the direct B_c meson production. This fact gives us additional opportunity to separate the contribution of the resolved-photon interaction process in B_c^* meson $\gamma\gamma$-production already at not very large energies $\sqrt{s_{\gamma\gamma}} = 20 - 50$ GeV.

Really, the generation of fixed energy $\gamma\gamma$-beams is very difficult problem. Now we may study $\gamma\gamma$-collisions at e^+e^-machines using the Weizsacker–Williams bremsstrahlung photon spectrum [15] or using the photon spectrum obtained by Compton back-scattering of the laser photons on high energy e^+e^- beams [16]. Fig. 6 shows the results of our calculation for B_c^* meson production cross section in e^+e^- collisions versus the e^+e^- center-of-mass energy $\sqrt{s}$. The curves in Fig.5 are obtained by folding $\gamma\gamma$ cross section with Weizsacker–Williams bremsstrahlung photon spectrum (lower curves) and with the spectrum of the back-scattered laser photons (upper curves). The cross section of B_c^* meson production from bremsstrahlung photons is very small at LEP energies but increases logarithmically with energy as the same Ref.[9]. We see that the contribution of the point-like hadronic component of the $c-$quark PSF becomes important only in the TeV energy range. In contrast, the cross section of B_c^* meson production from Compton back-scattered photons has a maximum at LEP energies. The energy dependence above $\sqrt{s} = 100$ GeV predicted by the model of the direct production [9] and by the resolved photon mechanism are very different. The cross sections obtained in Ref.[9], as well as in this paper for VMD and BH approaches, fall at $\sqrt{s} > 100$ GeV, but the B_c^* meson production cross section, which was calculated using PLH parametrization and taken into account NLO QCD corrections, speedily increases at $\sqrt{s} > 100$ GeV. So, at $\sqrt{s} = 1$ TeV one has $\sigma_{B_c^*} \sim 0.4$ pb. The values of the cross sections in the peak of $B_c(B_c^*)$ meson e^+e^--production are $\sigma_{B_c^*} \approx 0.2$ pb, $\sigma_{B_c} \approx 0.06$ pb. At the TeV energy region one has large contribution of the resolved photon interaction: $\sigma_{B_c^*} \approx 1$ pb, $\sigma_{B_c} \approx 0.3$ pb.

Based on photon structure function formalism we have calculated $B_c(B_c^*)$ meson production cross section in $\gamma\gamma$-collisions via partonic subprocess $c(\gamma)\gamma \to B_c(B_c^*)b$. It was shown that at the small energies this approach gives the same results for B_c^* meson cross sections as the direct leading order QCD calculation of the subprocess $\gamma\gamma \to B_c^* b\bar{c}$ at small energy. Howere, opposite to the direct QCD calculation we have obtained the increase of the $B_c(B_c^*)$ meson cross section at large energies. We have found also additional contribution to the B_c meson production connected with the nonperturbative fluctuations $\gamma \leftrightarrow J/\psi$. It was shown that charm content of the photon may be study experimentally in the $B_c(B_c^*)$ meson production already at the total energy 50 GeV in $\gamma\gamma$-collisions and at the total energy 200 GeV in e^+e^-collisions using Compton back-scattered photons. The discussed here $B_c(B_c^*)$ meson production mechanism can be used for prediction of the $B_c(B_c^*)$ meson production rates at high energies ep and $p\bar{p}$-colliders via partonic subprocess $cg \to B_c(B_c^*)b$ [17].

Authors thank A.K. Likhoded for useful discussions of the B_c-meson physics and E. Laenen for the valuable information about obtained results. This research was supported by the Russian Foundation of Basic Research (Grant 93-02-3545) and by State Committee on High Education of Russian Federation (Grant 94-6.7-2015).

References

[1] M.Derrick et al.(ZEUS Coll.), Phys.Lett. B322, 287(1994), B332, 228 (1994); T. Ahmed et al. (H1 Collaboration), Phys.Lett. B297, 205 (1992); Preprint DESY 94-153.

[2] E.Witten, Nucl.Phys. B120, 189 (1977); Ch.Berger and W.Wagner, Phys.Rep. 146, 1 (1987).

[3] D.Duke and J.Owens, Phys.Rev. D26, 1600 (1982); M.Dress and K.Grassie, Z.Phys. C28, 451 (1985); M.Drees and R.M.Godbole, Nucl.Phys. B339, 355 (1990).

[4] S.J.Brodsky et al., Phys.Lett. B93, 451 (1980); S.J.Brodsky and C.Peterson, Phys.Rev. D23, 2745 (1981).

[5] V.Barger, F.Halzen and W.Y.Keung, Phys.Rev. D25, 112 (1982).

[6] V.A. Saleev, Mod.Phys.Lett. A12, 1083 (1994); Yad.Fiz. 58, 501(1995); A.P. Martynenko and V.A. Saleev, Phys.Lett. B343, 381 (1995).

[7] V.A.Saleev, Yad.Fiz. 59(2), 1(1996), hep-ph 9502233.

[8] A.V.Berezhnoy, A.K.Likhoded and M.V.Shevlyagin, Preprint IHEP 94-82, Phys.Lett. B342, 351 (1995)

[9] K.Kolodziej, A.Leike and R.Rückl, Phys. Lett. B348, 219 (1995).

[10] B.Guberina, J.H.Kühn, R.D.Peccei and R.Rückl, Nucl.Phys. B174, 317 (1980).

[11] J.A.M.Vermaseren, FORM User's Guide, Nikhef-Amsterdam, 1990.

[12] M.Gluck, K.Grassie and E.Reya, Phys.Rev. D30, 1447 (1984).

[13] V.G. Kartvelishvili, A.K. Likhoded and V.A. Petrov, Phys.Lett. B72, 615 (1978); A.K. Likhoded, S.R. Slabospitsky and A.N. Tolstenkov, Yad.Fiz. 38, 1240 (1982).

[14] E.Laenen, S.Riemersma, J.Smith, W.J. van Neerven, Phys.Rev. D49, 5753 (1994); E.Laenen, private communication.

[15] C.F.Weizsäcker, Z.Phys. 88, 612 (1934); E.J.Williams, Phys.Rev. 45, 729 (1934).

[16] I.F.Ginzburg, G.L.Kotkin and V.I.Telnov, Nucl.Inst.Meth. 205, 47 (1983).

[17] V.A.Saleev, in preparation.

Figure captions.

1. Diagrams used to describe the partonic subprocess $c\gamma \to B_c(B_c^*)b$.

2. C-quark distributions in the photon. Curves 1-3 are respectively BH, VMD and PLH parametrizations.

3. Cross sections for $\gamma\gamma \to B_c^* X$ process versus the c.m. energy $\sqrt{s_{\gamma\gamma}}$. Curves 1 - 3 are respectively contributions of $c\gamma \to B_c^* b$ subprocess using BH, VMD and PLH parametrizations. The stars are the result of calculation $\gamma\gamma \to B_c^* b\bar{c}$ subprocess, which is taken from Ref.[8].

4. Energy distribution of B_c^* mesons at $\sqrt{s_{\gamma\gamma}} = 20$ GeV in the resolved photon interaction. The curves 1 and 2 are the same as Fig.3

5. Energy distribution of B_c^* mesons at $\sqrt{s_{\gamma\gamma}} = 100$ GeV in the resolved-photon interaction. The curves are the same as Fig.3.

6. Cross sections for $e^+e^- \to B_c^* X$ process versus the e^+e^- c.m. energy $\sqrt{s}$ with bremsstrahlung (lower curves) and with back-scattered laser (upper curves) photon spectra. The curves are the same as Fig.3.

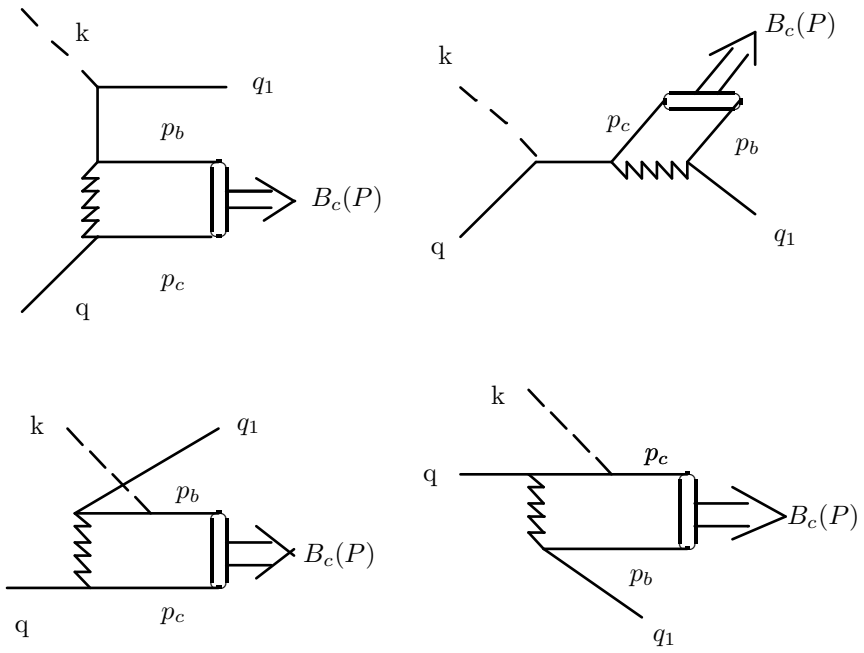

Fig. 1